Author Manuscript

Author Manuscript

Author Manuscript

Author Manuscript

HHS Public Access

Author manuscript

J Neurosci Methods. Author manuscript; available in PMC 2023 April 24.

Published in final edited form as:

J Neurosci Methods. 2021 February 01; 349: 109024. doi:10.1016/j.jneumeth.2020.109024.

Probing neural tissues at small scales: Recent progress of oscillating gradient spin echo (OGSE) neuroimaging in humans

Junzhong Xu[1,2,3,4,*]

[1]Vanderbilt University Institute of Imaging Science, Vanderbilt University Medical Center, Nashville, TN 37232, USA

[2]Department of Radiology and Radiological Sciences, Vanderbilt University Medical Center, Nashville, TN 37232, USA

[3]Department of Biomedical Engineering, Vanderbilt University, Nashville, TN 37232, USA

[4]Department of Physics and Astronomy, Vanderbilt University, Nashville, TN 37232, USA

Abstract

The detection sensitivity of diffusion MRI (dMRI) is dependent on diffusion times. A shorter diffusion time can increase the sensitivity to smaller length scales. However, the conventional dMRI uses the pulse gradient spin echo (PGSE) sequence that probes relatively long diffusion times only. To overcome this, the oscillating gradient spin echo (OGSE) sequence has been developed to probe much shorter diffusion times with hardware limitations on preclinical and clinical MRI systems. The OGSE sequence has been previously used on preclinical animal MRI systems. Recently, several studies have translated the OGSE sequence to humans on clinical MRI systems and achieved new information that is invisible using conventional PGSE sequence. This paper overviews the recent progress of the OGSE neuroimaging in humans, including the technical improvements in the translation of the OGSE sequence to human imaging and various applications in different neurological disorders and stroke. Some possible future directions of the OGSE sequence are also discussed.

Keywords

diffusion; oscillating gradient; diffusion time; MRI; microstructure; diffusion dispersion; size

Introduction

Diffusion MRI (dMRI) provides a unique means to characterize the microstructure of biological tissues non-invasively. Numerous dMRI methods, including diffusion tensor imaging (DTI) (Basser et al., 1994) and multi-compartment quantitative dMRI models

[*]**Corresponding author**: Address: Vanderbilt University, Institute of Imaging Science, 1161 21st Avenue South, AA 1105 MCN, Nashville, TN 37232-2310, United States. Fax: +1 615 322 0734. junzhong.xu@vanderbilt.edu (Junzhong Xu).

Author statement

Junzhong Xu: Conceptualization and Writing.

Declarations of interest

None.

Author Manuscript Author Manuscript Author Manuscript Author Manuscript

(Kaden et al., 2016; Zhang et al., 2012), have been widely used in neuroimaging for the diagnosis and assessment of treatment in various neurological disorders and stroke. It remains an active research topic nowadays to further develop and validate more advanced dMRI methods. Despite a large variety of different dMRI methods, the majority of dMRI acquisitions use the pulsed gradient spin echo (PGSE) sequence that was originally introduced by Stejskal and Tanner for diffusion measurements (Stejskal, 1965; Stejskal and Tanner, 1965). This method uses two pulsed diffusion gradients each with a duration of δ and separated by a time interval of Δ. If $\delta \ll \Delta$ (i.e., short pulse approximation), Δ is approximately the effective diffusion time t_{diff}, during which water molecules diffuse and constantly encounter barriers/obstacles that restrict/hinder diffusion. Such restrictions/hindrances reflect tissue microstructures such as the density and permeability of myelin sheaths and cell membranes, which in turns provides an opportunity to probe tissue status non-invasively. Therefore, diffusion time is one important factor for diffusion measurements because it determines the average number of interactions between water molecules and tissue microstructure.

In theory, different t_{diff} values can be achieved by simply adjusting Δ and δ. However, there are hardware constraints in practice that limit achievable $t_{diff} > 30$ ms particularly on human MRI systems. Because the root-mean-square displacement of diffusion is $l = \sqrt{2Dt_{diff}}$, typical diffusion measurements are more sensitive to length scale > 13 μm, which is much larger than typical axon and cell sizes in the central nervous system (CNS). To overcome the limitations of the PGSE sequence, the oscillating gradient spin echo (OGSE) sequence has been developed to achieve much shorter diffusion times with the presence of hardware constraints (Schachter et al., 2000; Tanner, 1979). The OGSE sequence replaces the pulsed gradients with oscillating gradients and the effective diffusion time t_{diff} is not dependent on the separation of two gradients (Δ) but is determined by the oscillating period T ($= 1/f$, the oscillating frequency). Although it is unclear how exactly t_{diff} is related to f, a shorter t_{diff} can generally be achieved using a higher f. This provides an opportunity for the OGSE sequence to probe much shorter diffusion times with hardware limitations.

Over the last two decades, the OGSE sequence has been widely used in preclinical studies to probe short diffusion times to reveal information at small length scales that are not available for the PGSE sequence. For examples, the OGSE sequence has been used in the measurement of surface-to-volume ratios of beads (Schachter et al., 2000) and cells (Xu et al., 2011b), probing intracellular structure variations during cell dividing (Xu et al., 2011b) and response to treatment (Colvin et al., 2011a; Xu et al., 2009b; Xu et al., 2012), enhancing imaging contrast to mouse brain tissues (Aggarwal et al., 2014; Aggarwal et al., 2012), estimating axon sizes (Drobnjak et al., 2016; Kakkar et al., 2018; Mercredi et al., 2017; Xu et al., 2014), and monitoring tumor response to treatment (Colvin et al., 2011b; Jiang et al., 2019a; Xu et al., 2012). Recently, other than using OGSE alone for short diffusion times, the combination of the OGSE and PGSE acquisitions has shown promise to probe more comprehensive microstructural information over a broader range of diffusion times, such as estimating mean cancer cell sizes and intracellular diffusion coefficients simultaneously (Jiang et al., 2017; Jiang et al., 2016a; Reynaud et al., 2016) This, in turn, provides a tool to monitor more specific tumor response to various treatments at both the cellular and

Author Manuscript Author Manuscript Author Manuscript Author Manuscript

subcellular levels. (Jiang et al., 2016b; Jiang et al., 2019a; Jiang et al., 2019b). However, these preclinical studies were usually performed on animal MRI systems with high gradient strengths G_{max} and slew rates SR that are usually not available on clinical MRI systems. It remains unclear if these preclinical findings can be directly translated to clinical imaging.

Recently, there is an increasing interest in translating the OGSE sequence to human MRI systems to characterize human tissues at smaller length scales. Due to the remarkable differences between preclinical and clinical hardware, the implementation of the OGSE sequence on human systems is significantly different from those reported on animal systems, including the acquisition protocols, detection sensitivity, and quantification methods. In this review paper, we will give an overview of the recent progress of OGSE neuroimaging in humans, including the technical translation of OGSE to human imaging and the recent applications of OGSE imaging in various diseases in patients. We will provide some opinions on possible future directions for OGSE imaging. Note that this review will focus on the practical aspects of OGSE imaging in humans only. Previous reviews have already covered the basics of the OGSE sequence including the frequency domain analysis (Gore et al., 2010) and the theories of the diffusion time dependency (Novikov et al., 2019).

Translation to human imaging

It is not trivial to translate preclinical imaging methods to clinical settings (Hormuth et al., 2019). This is particularly true for OGSE imaging. Because of $b \sim G^2/f^3$, achieving a higher frequency f (i.e., a shorter t_{diff}) while keeping a reasonable b value requires a stronger gradient strength G and a fast SR, both of which are very limited to human systems. To overcome this problem, several efforts have been made to develop new gradient coils and optimize the OGSE sequence while both of which require further improvements such as gradient calibration and deriving new quantification models.

Hardware: Gradients

The typical G_{max} and SR are $\leqslant$ 80 mT/m and $\leqslant$ 200 T/m/s, respectively, for most clinical MRI systems. Because G_{max} on preclinical systems is usually at least fivefold larger (e.g., $\geqslant$ 400 mT/m), this results in a very limited achievable f and t_{diff} on clinical MRI systems. Moreover, because the OGSE sequence usually maximizes the usage of gradients, the duty cycle of the gradient amplifier becomes a limiting factor that requires a larger TR and hence effectively increases the total scan time. The total duration of all gradient lobes on one side of the refocusing RF pulse is usually long (e.g., > 30 ms) for the OGSE acquisitions on clinical MRI systems so that this results in a long echo time (TE) typically ~ 110 ms which reduces the signal-to-noise ratios (SNR). Despite these disadvantages, several studies have reported the implementation of the OGSE imaging on current human systems of major MRI vendors. Table 1 summarizes the representative OGSE protocols and hardware in some previous OGSE human imaging studies. Most OGSE studies to date can only probe $f \leqslant 60$ Hz with a relatively lower b value < 450 s/mm^2. However, the high-performance, head-only gradient coil insert developed recently by Tan et al. significantly enhances the ability to probe f up to 100 Hz, corresponding to an effective $t_{diff} \approx 2.5$ ms (Tan et al., 2020), which

Author Manuscript Author Manuscript Author Manuscript Author Manuscript

opens an avenue to push the limit of detection sensitivity to much shorter length scales in humans.

Pulse sequence

The early OGSE imaging studies used either sine- or cosine-modulated gradient waveforms. Intuitively, the cosine waveform provides a shorter t_{diff}. In theory, the frequency domain analysis (Callaghan and Stepisnik, 1995; Stepisnik, 1981) suggests that cosine waveforms create encoding (sampling) spectra $|F(\omega = 2\pi f)|^2$ consisting of Dirac delta functions at specified frequencies, which is ideal to sample diffusion spectra $D(\omega)$ for comprehensive microstructural information. For this reason, cosine waveforms are widely used in preclinical OGSE studies on animal MRI systems, despite that it provides one-third of b values compared with the sine waveforms. However, cosine waveforms do not maximize the usage of the whole capacity of gradient coils so that the achievable b_{max} and f_{max} are not optimal. To overcome this, a cosine-modulated trapezoidal waveform (i.e., trapezoid-cosine) was suggested to maximize the usage of gradients (Van et al., 2014). Fig. 1 shows the comparison of the gradient waveforms and corresponding encoding frequency spectra $|F(\omega)|^2$ of the cosine and trapezoid-cosine waveforms. The trapezoid-cosine waveform always uses higher or equal gradients compared with the cosine waveform, while their $|F(\omega)|^2$ only differ slightly. This ensures the trapezoid-cosine waveforms provides higher b values than the cosine waveform with the same hardware. Specifically, the b of the apodised cosine waveform is given by

$$b = \left(\gamma^2 G_{max}^2 n\right)/\left(4\pi^2 f^3\right)\left(1 - \frac{1}{8n}\right) \quad [1]$$

while b of the trapezoid-cosine waveform is

$$b = \gamma^2 G_{max}^2\left[(t_r + t_p)^2(\Delta - (t_r + t_p)/3) + t_r^3/30 - (t_r + t_p)t_r^2/6\right] \quad [2]$$

where γ is the gyromagnetic ratio, n is the number of oscillations in each gradient, t_r is the gradient rise time (i.e., the time allows the gradient increases from 0 to the maximum), and t_P is the duration time of the first gradient plateau. The exact enhancement in b values is hardware dependent. For example, if G_{max} = 80 mT/m, t_r= 0.9 ms, δ= 40 ms, and f = 25 Hz, b_{max}= 1130 s/mm^2 for trapezoid-cosine waveform, which is 52% higher than b_{max} = 745 s/mm^2 for the cosine waveform. Presumably due to the ability to maximize b while keeping similar frequency sampling spectra $|F(\omega)|^2$, the trapezoid-cosine waveform has been widely used in almost all recent OGSE imaging studies in humans as shown in Table 1.

Quantification

In addition to the popular DTI, it remains an active research topic to quantitatively characterize tissue microstructural properties such as cell size, density, and diffusivities using dMRI non-invasively. To this end, analytical expressions are usually needed to link dMRI signals to the dMRI sequence parameters and underlying biophysical properties. For the PGSE sequence, analytical equations to predict dMRI signals in a few regular geometries

Author Manuscript Author Manuscript Author Manuscript Author Manuscript

(i.e., planes, cylinders, and spheres) were reported back in the ’70s (Neuman, 1974). For the OGSE sequence, the analytical equations were first derived based on the velocity correction function for infinitely long, ideal OGSE sequences (Stepisnik, 1993). However, there are many limiting factors on OGSE sequences in realistic experiments such as the finite duration of δ and Δ, and limited SR. The δ and the number cycles affect the OGSE results (Novikov and Kiselev, 2011; Sukstanskii, 2013). The choice of appropriate Δ is sometimes overlooked in OGSE experiments but it can play an importantly role to modulate $|F(\omega)|^2$ (Baron and Beaulieu, 2014). Based on the realistic gradient waveforms with all practical parameters, analytical expressions to predict dMRI signals have been derived for sine and cosine waveforms (Xu et al., 2009a) and the square and general sine-modulated trapezoidal waveforms (Ianus et al., 2013). For the trapezoid-cosine waveforms that are widely used in OGSE imaging studies in humans, the analytical expressions were reported recently (Xu et al., 2020). Because the analytical expressions are usually very complicated and long, we do not show the equations here but encourage readers to refer to the previous papers for details. Note that the above analytical equations have been used in several studies to estimate e.g., cell sizes and diffusivities with comprehensive validations using simulations *in silico*, cell cultures *in vitro*, and animals *in vivo* (Jiang et al., 2017; Jiang et al., 2016a; Jiang et al., 2020; Xu et al., 2020).

It is worth mentioning that the above analytical equations for OGSE sequences are based on a Gaussian approximation for the phase distribution (Stepisnik, 1993). However, studies have shown that this approximation is valid with a broad range of f and b values (Ianus et al., 2013; Xu et al., 2009a). For example, a comparison of simulated and analytical signal echo attenuations suggests < 2.9% of discrepancies occur when b values increase up to 5000 mm^2/s (Xu et al., 2009a). Because b values are always limited to human MRI scanners, this Gaussian approximation is not expected to affect the accuracy of analytical equations for OGSE sequences. Moreover, recent analytical equations of trapezoid-cosine waveforms were derived based on the realistic waveforms performed on the human MRI scanners (Xu et al., 2020), which in turn further increases the accuracy of analytical equations to descript realistic signals in measurements.

Calibration

Gradient calibration is essential for any dMRI measurements but is sometimes overlooked. In addition to the gradient nonlinearity that affects all diffusion sequences (Malyarenko et al., 2014), the OGSE sequence is so far not a standard sequence on clinical systems so it requires more attenuation on calibration. One of the most attractive applications of the OGSE sequence is the ability to probe much shorter t_{diff} and smaller length scales, so the diffusion time dependence is key information. Therefore, it is essential to calibrate the sequence and hardware to ensure any dMRI signal variations across different t_{diff} are caused by underlying biophysical properties, not by hardware or sequence inconsistency among different t_{diff} values.

To complicate matters, previous studies have reported a few unique calibration issues related to the OGSE sequence that need extra attention, including

Author Manuscript Author Manuscript Author Manuscript Author Manuscript

i. **Amplifier response**. If very high gradient frequencies are acquired with strong gradient strengths and slew rates, the gradient amplifier may lose linear response, resulting in significantly biased ADCs (Xu et al., 2011b).

ii. **Mechanical vibration**. For certain gradient and MRI systems, the OGSE sequence could result in remarkable mechanical vibrations only at a certain diffusion gradient frequency, which can cause serious motion artifacts. For example, severe mechanical vibrations were found in studies of both phantoms and tissues *in vivo* at 150 Hz only in a wide frequency range of 50 – 250 Hz using a gradient insert on a 4.7 Tesla preclinical scanner (Xu et al., 2012).

iii. **Signal drift**. The dMRI signal drifts may become more severe during the OGSE acquisitions presumably due to the gradient coil heating caused by the heavy usage of gradients. This effect could be minimized by using dynamic stabilization during acquisitions (Xu et al., 2020) and the dMRI signal drift correction (Vos et al., 2017).

Therefore, it is important to perform comprehensive calibration of the OGSE sequence to ensure every gradient axis is well-calibrated with the OGSE sequence. Possible approaches include the use of well-established, temperature-controlled phantoms with known ADC values such as ice-water phantoms (Chenevert et al., 2011) and alkane phantoms with different viscosities (Maekawa et al., 2018). Fiber phantoms have been used to evaluate the accuracy of the OGSE imaging for estimating surface-to-volume ratio (S/V), which can also serve to evaluate the accuracy of OGSE acquisitions on clinical MRI systems (Lemberskiy et al., 2017).

New information obtained using OGSE

OGSE dMRI signals with short diffusion times

It is well-known that t_{diff} plays an important role in restricted diffusion systems and dMRI signals vary with t_{diff} (Tanner and Stejskal, 1968). dMRI signals with different t_{diff} values are sensitive to different length scales and hence convey different microstructural information. This was observed in brain cancer studies in rodents that OGSE dMRI signals with smaller t_{diff} provides an increased contrast and shows more spatial heterogeneity inside brain tumors (Colvin et al., 2008). By contrast, the OGSE sequence with shorter t_{diff} have been found to diminish the imaging contrast of stroke lesions in patients (Baron et al., 2015; Boonrod et al., 2018). Although a reduced contrast may not be desirable for diagnosis, this behavior provides new insights for better understanding of the contrast mechanism of dMRI in stroke (Baron et al., 2015).

Diffusion time-dependent DTI

In addition to the direct usage of OGSE dMRI signals with short diffusion times, it is of great interest to apply the OGSE sequence to detect the t_{diff} dependence of diffusion tensor imaging (DTI) metrics, such as fractional anisotropy (FA), mean diffusivity (MD), axial diffusivity (AD), and radial diffusivity (RD). Previously, the t_{diff} dependence was not observed in human DTI studies using the PGSE sequence only, such as the DTI of normal

Author Manuscript Author Manuscript Author Manuscript Author Manuscript

human brains showed no significant changes with the t_{diff} range of 8 – 80 ms (Clark et al., 2001). Presumably, this is because these measurements were acquired using the PGSE sequence with t_{diff} not short enough to allow the movements of water molecules to be appear less restricted. The use of the OGSE sequence pushes the limits to shorter t_{diff} and hence gleans new information at smaller scales that are invisible in typical PGSE imaging. The OGSE DTI study was first performed in a fixed monkey brain (Xu et al., 2010) and later applied to rats (Kershaw et al., 2013) and human (Baron and Beaulieu, 2014) brains *in vivo*. These studies found that DTI metrics showed a t_{diff} dependence in most brain regions. In general, FA decreases with shorter t_{diff} while MD, AD, and RD increase. Such a t_{diff} dependence reveals additional microstructural information that is not achievable by the PGSE sequence alone. For example, this dependence suggests the existence of diffusion restriction in the laminated keratin layers within the cyst, which is not revealed by the PGSE sequence alone (Andica et al., 2018).

Diffusion dispersion with frequency

The diffusion spectrum $D(f)$ over a broad range of frequencies and t_{diff} is desirable to characterize comprehensive information on tissue microstructure (Parsons et al., 2006). However, the exact dependence of $D(f)$ on f is determined by the specific f range (Reynaud, 2017). In the high frequency (short t_{diff}) regime, Mitra's equation is valid so $D(f) \sim f^{-1/2}$ (Novikov and Kiselev, 2011; Xu et al., 2011b). In the low frequency (long t_{diff}) regime, there is a power-law relationship between ADC and f as $\mathrm{ADC} = \mathrm{ADC}_0 + \Lambda \cdot f^{\theta}$ (Burcaw et al., 2015; Novikov et al., 2014), where the constant Λ is defined as diffusion dispersion rate. This relationship has been observed in OGSE imaging in healthy human subjects with fitted $\theta = 0.5$ and f from 0 (PGSE) to 60 Hz (Arbabi et al., 2020). However, this study included ADCs achieved by PGSE as $\mathrm{ADC}(f = 0)$ in the ADC spectrum analyses, but it remains unclear if this approximation is valid in practice. The PGSE and OGSE have very different gradient waveforms and power spectra, and they have different sensitivities to flow (Wu and Zhang, 2017) and background gradients (Hong and Thomas Dixon, 1992). The differences between PGSE and OGSE signals may not arise just from diffusion time dependence but also from other confounding effects. Although such differences have been found useful to assess the age and sex differences in the human corpus callosum (Tétreault et al., 2020) and to assess neonatal hypoxia-ischemia (Gao et al., 2020), it is plausible to reduce the complexity of ADC spectrum analyses by excluding PGSE data and focused on ADCs achieved by OGSE only (Aggarwal et al., 2014; Aggarwal et al., 2012; Wu et al., 2014a; Xu et al., 2016; Xu et al., 2012). This ensures to minimize the influences of confounding effects. Because the achievable f in the OGSE acquisitions are usually remarkably limited by available hardware, particularly on clinical MRI systems, only a narrow range of f can be acquired in practice. In such a narrow range, the t_{diff} dependence of ADC on f was found to be approximated as a linear function for $f > 0$ (i.e., excluding a PGSE acquisition), i.e., $\mathrm{ADC} = \mathrm{ADC}_0 + \mathrm{DDR} \cdot f$, where DDR is the linear diffusion dispersion rate that describes the rate that ADC increases with t_{diff} approximately in a linear manner (Xu et al., 2016; Xu et al., 2012). Note that some groups use $\Delta_f ADC$ to indicate the same concept (Aggarwal et al., 2014; Aggarwal et al., 2012; Wu et al.,

Author Manuscript Author Manuscript Author Manuscript Author Manuscript

2014a). Fig.2 shows linear t_{diff} dependence in six representative human brain regions with f from 20 to 100 Hz acquired *in vivo* (Tan et al., 2020). Although it still requires further investigation on how to include PGSE data (particularly those with different t_{diff} values) in the ADC spectrum analyses, either power law or approximated linear relation seem able to describe the t_{diff} dependence because of the narrow ranges of f achievable in practice. However, the approximated linear dependence has been found to provide more reliable data fitting e.g., in cell size estimation in tumors using the OGSE sequence (Jiang et al., 2016a). Even excluding PGSE data, the underlying biophysical meaning of DDR needs more investigation. Evidence has suggested DDR contains microstructural information such as the sizes of intrinsic microstructure (Li et al., 2015) so that it can be used as a simple and fast indicator of cell or axon sizes. For example, DDR has been used to monitor rodent tumor response to treatment (Xu et al., 2012), to enhance imaging contrast to of mouse hippocampus and cerebellum (Aggarwal et al., 2014; Aggarwal et al., 2012; Wu et al., 2014a), and to show correlation with mean axon diameters in fixed rat spinal cords and human corpus callosum *in vivo* (Xu et al., 2016). Note that the previously reported DDRs in animals and humans are different, which might attribute to different neurite sizes. However, further investigation is required.

Another advantage of DDR is its fast acquisition. In theory, DDR can be achieved using a minimum of two ADC measurements, although more ADCs may enhance the data fitting. A recent study has optimized a fast (~ 6 mins) protocol with one OGSE frequency and one PGSE (Arbabi et al., 2020), suggesting potential for clinical applications.

Intracranial neuroimaging applications

To date, the majority of the reported OGSE applications focus on brain imaging. With much shorter t_{diff}, new information can be achieved which may provide new insights into the diagnosis of various diseases or assist in better understanding of the biophysical mechanism of imaging metrics. The intracranial OGSE imaging has been applied to patients with stroke (Baron et al., 2015; Boonrod et al., 2018), NPH (normal pressure hydrocephalus) (Irie et al., 2019), epidermoid cysts (Andica et al., 2018), multiple sclerosis (Li et al., 2017), and brain cancer (Xu et al., 2017). In this review, we will focus on the new information achieved with the OGSE sequence in stroke and NPH.

Stroke

dMRI has been used daily as a sensitive method for the diagnosis of stroke. It is well known for decades that ADC decreases after stroke, but the underlying biophysical mechanism remains elusive. Several theories have been developed to explain the reduction of ADC in strokes, such as brain cell swelling (cytotoxic edema) (Warach et al., 1995) and neurite beading (Budde and Frank, 2010). dMRI has been used daily for the diagnosis of stroke and almost all acquisitions are using the PGSE sequence with relatively long t_{diff}. This limits dMRI to convey microstructural information averaged over relatively long length scales, which in turn makes it challenging to entangle signal contributions from different sources in stroke. If a short t_{diff} could be used and push the detection sensitivity to shorter length scales, more microstructural information could be achieved which may assist in elucidating

Author Manuscript Author Manuscript Author Manuscript Author Manuscript

the underlying biophysical mechanism of ADC reduction in stroke. Does et al. first applied the OGSE imaging in globally ischemic rat brains (Does et al., 2003) and Wu et al. reported the use of the OGSE imaging in hypoxia-ischemia injured mouse brains (Wu et al., 2014a). Both studies observed that the contrast between ischemic lesions and normal tissues reduces at shorter t_{diff}. These findings were confirmed by Baron et al. in the OGSE imaging in stroke patients (Baron et al., 2015). As shown in Fig.3, the imaging contrast of ischemic stroke lesions reduces with shorter t_{diff} at multiple time points post onset. In white matter, the PGSE MD maps with $t_{diff} = 40$ ms show hypointense lesions, but these lesions are nearly isointense in OGSE MD maps. In gray matter, there are no significant differences between PGSE and OGSE. Confirmed with computer simulations, Baron et al. suggested that the reduction of ADC in white matter in stroke is due to neurite beading and axonal swelling. Recently, similar findings were also reported in cerebral infarctions in patients (Boonrod et al., 2018).

Interestingly, a preclinical study (Wu et al., 2019) found out that OGSE MRI, particularly DDR, provides much higher sensitivity to subtle hypoxia-ischemia (HI) brain tissue damages compared with PGSE in a mouse model. Specifically, they found more significant increases (average 64.8% and 48.9% ipsilateral hippocampal CA1 and cortical regions vs. the contralateral side) in DDR than the modest decrease in PGSE ADC's (average 6.5% and 2.7% decreases). More recently, similar findings have been reported in neonates with hypoxic-ischemic encephalopathy (HIE) using clinical MRI scanners (Gao et al., 2020). These observations suggest, the t_{diff} dependence achieved using OGSE may provide a more sensitive indicator to the microstructural changes in stroke. However, as PGSE already provides high sensitivity to stroke, OGSE imaging with shorter t_{diff} may not be a replacement for stroke diagnosis but may provide new insights into stroke lesions that can assist in elucidating the biophysical contrast mechanism of ADC in stroke.

NPH (normal pressure hydrocephalus)

Normal pressure hydrocephalus (NPH) is a clinical symptom complex caused by the build-up of cerebrospinal fluid (CSF) without increasing CSF pressure (Adams et al., 1965). Previous studies have used DTI to characterize the mechanical compression of white matter presumably due to ventricular enlargement (Assaf et al., 2006; Hattori et al., 2011). They found AD increased (+10%) and RD decreased (-25%) in the patient white matter close to ventricles, particularly in the corticospinal tract (CST). Although these findings were consistent with the theory of mechanical compression, it remains unclear if the variations of DTI metrics reflect such underlying pathological changes because DTI is usually affected by many tissue properties simultaneously. If shorter t_{diff} can be achieved, additional microstructural information can be obtained which may assist in better interpretation of DTI data in NPH. Irie et al. recently reported the OGSE imaging in NPH patients with f up to 30 Hz (effective $t_{diff} \approx 8.3$ ms) (Irie et al., 2019). They observed that both AD and RD increase with shorter t_{diff} in CST and hence defined ΔADC, the ADC differences between the short and long t_{diff} i.e., $\Delta\text{ADC} = \text{ADC}(t_{diff}^{short}) - \text{ADC}(t_{diff}^{long})$ as in (Gao et al., 2020). They found ΔADC's in NPH patients are significantly lower than in those in healthy subjects. This trend is opposite to the change of cerebral infarction (Boonrod et al., 2018). A possible

Author Manuscript Author Manuscript Author Manuscript Author Manuscript

explanation is that "*nerve fibers are compressed and stretched straight in NPH*". Although this hypothesis needs further validation, the use of OGSE and t_{diff} dependence provide additional sensivity to subtle tissue changes in NPH patients, which serve a new imaging biomarker for future NPH imaging.

Extracranial neuroimaging applications

There is increasing interest in applying the OGSE sequence in extracranial applications, such as spinal cord (By et al., 2019), peripheral nerve (Li et al., 2016), liver (Jiang et al., 2020), head and neck cancer (Iima et al., 2019), and breast cancer (Xu et al., 2020). We here will focus on OGSE neuroimaging in the spinal cord and peripheral nerve.

Spinal cord

By et al. reported the first application of the OGSE imaging in the human spinal cord *in vivo* with t_{diff} from 8.77 ms to 66.7 ms (By et al., 2019). Unlike that AD dominates the t_{diff} dependence in the brain, AD in the spinal cord of healthy subjects appears to be negligibly affected with t_{diff} with ≤1.53% changes across all t_{diff} acquired. This is very different from the significant t_{diff} dependent AD in the brain (Baron and Beaulieu, 2014). The underlying mechanism remains unclear. By contrast, RD shows a 37% mean increase when t_{diff} decreases from 66.7 ms (acquired using the PGSE sequence) to 8.77 ms (using the OGSE sequence). This results in a 12.9% decrease in FA. By et al. also applied the OGSE sequence in the spinal cord of multiple sclerosis patients. Fig. 4 shows the RD maps of the cervical spine for representative control and MS patient. A larger increase (46.5%) in RD in the MS patient is observed with the OGSE sequence, in comparison to 40.7% with the PGSE sequence. This is opposite to the findings in stroke, in which the imaging contrast decreases with shorter t_{diff}. This indicates an increased sensitivity to pathological variations in MS using the OGSE sequence with shorter t_{diff}. The reason why OGSE increases the sensitivity to MS remains unclear, but a possible explanation is that the demyelination in MS causes a larger extra-axonal space with an increased restriction size (spacing between axons). Because OGSE with shorter t_{diff} is more sensitive to this subtle change in restriction sizes, RD obtained with OGSE shows a more significant increase, resulting in an increased sensitivity to MS lesions.

Peripheral nerve

Peripheral nerves refer to parts of the nervous system outside the brain and spinal cord. They transmit motor/sensory information between the central nervous system (CNS) and other parts of the body. Peripheral nerve injury can disrupt this transmission, resulting in a variety of symptoms (e.g., pain, weakness). The axon sizes in many peripheral nerves are usually much larger than those in the CNS, making it suitable to be estimated using typical dMRI even on clinical MRI systems. Because the OGSE sequence probes shorter t_{diff}, it can assist in better estimating the mean axon size in peripheral nerves. Li et al. reported the first application of estimating the mean axon size in the human sciatic nerve *in vivo* using the OGSE sequence (Li et al., 2016). With the IMPULSED model (Jiang et al., 2016a), they fitted the mean axon diameter of 9.8±0.9 μm and mean axonal signal fraction 47±4%,

Author Manuscript Author Manuscript Author Manuscript Author Manuscript

consistent with previous histological findings (Ikeda and Oka, 2012). Because diseases may affect certain axon populations (e.g. small sensory fibers damaged in diabetic neuropathy), this technique may provide more specific information on neural injury in peripheral nerves, compared with conventional DTI.

Possible future directions

Despite several successful applications of the OGSE sequence on clinical MRI systems, it is still at the very early stage of implementing OGSE for human imaging. Here, we provide a few thoughts on possible future directions to further improve the OGSE imaging in humans.

Hardware

As mentioned above, the majority of the OGSE neuroimaging was performed using the regular clinical MRI systems with e.g., gradient strengths G_{max} up to 80 mT/m and slew rates SR up to 200 T/m/s. This typically limits the achievable f up to 60 Hz, i.e., with $t_{diff} \sim 4$ ms. The recent development of the high-performance, head-only gradient coils pushes the limits to $t_{diff} \sim 2.5$ ms and $b = 450$ s/mm^2, which opens an avenue to probe much smaller length scales in human brains. With the rapid development of more cutting-edge gradient coils for humans, even stronger G_{max} and SR can be achieved. For example, $t_{diff} \sim 2$ ms and $b \sim 420$ s/mm^2 could be achieved theoretically with $G_{max} = 300$ mT/m and SR = 200 T/m/s in multi-directional dMRI measurements using the human connectome coil (Setsompop et al., 2013). The connectome 2.0 coil under development could theoretically probe $t_{diff} \sim 1.25$ ms and $b \sim 473$ s/mm^2 with $G_{max} = 500$ mT/m and SR = 600 T/m/s. However, due to hardware limitations and physiological constraints (such as peripheral nerve stimulation and cardiac stimulation), maximum G_{max} and SR are not likely to be achievable simultaneously (Setsompop et al., 2013). This in turn limits the ability of OGSE to achieve the shortest t_{diff} possible with hardware constraints. It is likely the achievable t_{diff} ranges will be machine dependent. However, OGSE achievable shortest t_{diff} should be much shorter than those achievable by PGSE, because the latter should be always larger than the sum of the gradient duration δ and the duration of the 180° refocusing RF pulse. Therefore, the recent hardware developments will significantly improve the ability of the OGSE sequence to probe much shorter length scales.

Note that the above calculations of maximum b values are based on arbitrary directions. It is worth mentioning the maximum possible b values in OGSE measurements also depend on acquisition strategies with the same hardware limitations. For example, DTI measurements using the minimal six-direction icosahedral scheme can allow two diffusion gradients to be on simultaneously, leading to doubled maximum b values. If only MD is desired, the four-direction tetrahedral scheme can result in tripled maximum b values (Conturo et al., 1996). Another approach of circularly polarized oscillating gradient sequence was developed to extend achievable diffusion times with gradient strength limits for DTI measurements as well (Lundell et al., 2015).

Author Manuscript Author Manuscript Author Manuscript Author Manuscript

Acquisition

There are a few drawbacks in OGSE acquisitions that require further improvements. First, the limited gradient strengths confine the shortest diffusion time achievable. Second, the gradient duty cycle limited longer TR's result in longer scan time. Moreover, the relatively long gradient durations (typically δ > 30 ms) and echo times (typically TE > 100 ms) significantly limit the SNR of OGSE acquisitions, particularly on higher field strength when T_2 is shorter. There are several efforts to tackle these issues. The integration of multiband can remarkably reduce TR and accelerate whole-brain OGSE acquisitions (Xu et al., 2019). However, the inclusion of multi-band will further increase TE and reduce SNR. Recently, Wu et al. reported a diffusion-prepared 3D gradient and spin-echo sequence (GRASE) to tackle both issues by reducing the scan time by a factor of 1.38 and increasing the SNR by a factor of 1.74 – 2.27 compared (Wu et al., 2020). Hennel et al. developed a modified trapezoid-cosine gradient waveform and achieved a range of 30 – 75 Hz with a b-value of nearly 1000 s/mm^2 in DTI measurements in human white matter by using a high-performance gradient insert (Hennel et al., 2020). Moreover, it is possible to further accelerate OGSE acquisitions by combining other emerging techniques such as multi-slab (Engström and Skare, 2013) and compress sensing (Wu et al., 2014b). We emphasize that OGSE is one type of dMRI so that it will benefit from the extensive improvements of dMRI acquisitions.

Biophysical mechanism

One of the main benefits of the OGSE sequence is to achieve much shorter diffusion times t_{diff} so that a t_{diff} dependence can be obtained to characterize the microstructure of tissues (Xu et al., 2011a). The biophysical theories of t_{diff} dependence of dMRI have been investigated comprehensively, particularly in the short and long t_{diff} ranges (Mitra et al., 1992; Novikov et al., 2011; Novikov et al., 2019; Novikov et al., 2014; Novikov et al., 2018). However, biophysical tissues are very complex and heterogeneous so that the exact t_{diff} dependence varies with t_{diff} itself. In another word, the rates of ADC dependence on t_{diff} are different in different t_{diff} ranges. Therefore, it is important to determine in which t_{diff} range the experiments could achieve. For example, f up to 200 Hz (i.e., t_{diff} ~ 1.25 ms) is considered as *short* for tumors with cancer cell size ~ 16 μm. This provides an opportunity to fit cell size reliably (Jiang et al., 2017; Jiang et al., 2016a; Jiang et al., 2016b). By contrast, the same f up to 200 Hz is considered as *long* for nerves with axon sizes ~ 2 μm, with which small axon sizes and transverse intra-axonal diffusivities cannot be estimated reliably (Xu et al., 2014). To complicate matters, the variations of tissue during disease progression or response to intervention may change microstructure as well as the t_{diff} dependence. Hence, it is important to investigate the exact t_{diff} dependence for certain combinations of experimental parameters, tissue types, and interventions. This will affect the achievable t_{diff} ranges in low, intermediate, or long time regimes, which may determine the data interpretation and analyses.

Another controversial topic is the effective diffusion time t_{diff} for the OGSE sequence, i.e., how to convert f to t_{diff}. Intuitively, the effective t_{diff} of the OGSE sequence should be smaller than the period $(1/f)$ of sine-modulated waveforms or a half period of cosine-

Author Manuscript Author Manuscript Author Manuscript Author Manuscript

modulated waveforms, i.e., the total duration of a pair of encoding and decoding diffusion gradients. However, this is similar to the violation of the short pulse approximation in the PGSE sequence so that the exact t_{diff} is uncertain. Theoretical analyses suggest that there may not be a single t_{diff} in this case (Fordham et al., 1996), but several OGSE studies both in animals and humans defined effective $t_{diff} = 1/(4f)$ for cosine-modulated waveforms (Baron and Beaulieu, 2014; Does et al., 2003; Parsons et al., 2006; Xu et al., 2011b). This relationship was validated in packed spheres (Schachter et al., 2000), cell cultures (Xu et al., 2011b), and fixed animal nerves (Portnoy et al., 2013). However, a recent fiber phantom study suggested $t_{diff} = 9/(64f)$ with a validation using other MRI modalities (Lemberskiy et al., 2017). One possible explanation of the discrepancy may be the different length scales that result in different t_{diff} ranges. The fiber phantom study used fibers with a diameter of 17 μm combined with the relative loose packing resulting in a short t_{diff} range. By contrast, the t_{diff} was in the long time range becaure of the small nerves with sizes of < 2 μm (Portnoy et al., 2013). This suggests again that it is essential to first determine in which t_{diff} range the experiments are and then the appropriate models can be used.

Perfusion is another confounding effect. Due to the differences in gradient waveforms, the OGSE sequence is much less susceptible to blood perfusion than the PGSE sequence. Although this effect is small in the brain presumably due to a small cerebral blood volume fraction, perfusion plays an important role in e.g., the liver in which perfusion is significant (Jiang et al., 2020). Without correcting for this effect, the ADCs obtained using the PGSE sequence could be mistakenly higher than those obtained using the OGSE sequence, which violates the t_{diff} dependence theory (Jiang et al., 2020). In addition to the appropriate b ranges and corrections in data analyses, modified OGSE sequences could be helpful to address this issue (Wu and Zhang, 2017).

More applications in diseases

Studies have found the OGSE sequence shows significant advantages in human cancer imaging (Bongers et al., 2018; Iima et al., 2019; Xu et al., 2020). For neuroimaging, although the OGSE sequence provides additional information to elucidate the biophysical mechanism of dMRI in stroke, the reduced imaging contrast suggests that it may not be suitable for the diagnosis of stroke (Baron et al., 2015; Boonrod et al., 2018). However, the increased imaging contrast in multiple sclerosis in the spinal cord suggests that the OGSE sequence might be suitable for practical MS imaging (By et al., 2019). Therefore, it is of interest to further implement the OGSE sequence in different diseases to investigate if it provides any advantages. Currently, we are still at the very early stage of this implementation.

Conclusion

The OGSE sequence can probe much shorter diffusion times and smaller length scales with the presence of hardware limitations on clinical MRI systems. Recent progress of the OGSE imaging in humans has shown that it provides an opportunity to provide new microstructural information that is invisible using the conventional PGSE sequence. Further development

Author Manuscript Author Manuscript Author Manuscript Author Manuscript

and more applications are necessary to enable the OGSE sequence as a useful tool in daily clinical imaging.

Acknowledgment

The author was supported by NIH grants R01CA109106 and UG3CA232820.

References

Adams RD, Fisher CM, Hakim S, Ojemann RG, Sweet WH. Symptomatic occult hydrocephalus with "normal" cerebrospinal-fluid pressure. A treatable syndrome. . The New England journal of medicine, 1965; 273: 117–26. [PubMed: 14303656]

Aggarwal M, Burnsed J, Martin LJ, Northington FJ, Zhang J. Imaging neurodegeneration in the mouse hippocampus after neonatal hypoxia-ischemia using oscillating gradient diffusion MRI. Magnetic resonance in medicine, 2014; 72: 829–40. [PubMed: 24123409]

Aggarwal M, Jones MV, Calabresi PA, Mori S, Zhang J. Probing mouse brain microstructure using oscillating gradient diffusion MRI. Magnetic resonance in medicine, 2012; 67: 98–109. [PubMed: 21590726]

Andica C, Hori M, Kamiya K, Koshino S, Hagiwara A, Kamagata K, Fukunaga I, Hamasaki N, Suzuki M, Feiweier T, Murata K, Arakawa A, Kondo A, Akiyama O, Aoki S. Spatial Restriction within Intracranial Epidermoid Cysts Observed Using Short Diffusion-time Diffusion-weighted Imaging. Magnetic resonance in medical sciences : MRMS : an official journal of Japan Society of Magnetic Resonance in Medicine, 2018; 17: 269–72. [PubMed: 29129844]

Arbabi A, Kai J, Khan AR, Baron CA. Diffusion dispersion imaging: Mapping oscillating gradient spin-echo frequency dependence in the human brain. Magnetic resonance in medicine, 2020; 83: 2197–208. [PubMed: 31762110]

Assaf Y, Ben-Sira L, Constantini S, Chang LC, Beni-Adani L. Diffusion tensor imaging in hydrocephalus: initial experience. AJNR. American journal of neuroradiology, 2006; 27: 1717–24. [PubMed: 16971621]

Baron CA, Beaulieu C. Oscillating gradient spin-echo (OGSE) diffusion tensor imaging of the human brain. Magnetic resonance in medicine, 2014; 72: 726–36. [PubMed: 24142863]

Baron CA, Kate M, Gioia L, Butcher K, Emery D, Budde M, Beaulieu C. Reduction of Diffusion-Weighted Imaging Contrast of Acute Ischemic Stroke at Short Diffusion Times. Stroke, 2015; 46: 2136–41. [PubMed: 26152297]

Basser PJ, Mattiello J, LeBihan D. Estimation of the effective self-diffusion tensor from the NMR spin echo. Journal of magnetic resonance. Series B, 1994; 103: 247–54. [PubMed: 8019776]

Bongers A, Hau E, Shen H. Short Diffusion Time Diffusion-Weighted Imaging With Oscillating Gradient Preparation as an Early Magnetic Resonance Imaging Biomarker for Radiation Therapy Response Monitoring in Glioblastoma: A Preclinical Feasibility Study. International journal of radiation oncology, biology, physics, 2018; 102: 1014–23. [PubMed: 29429801]

Boonrod A, Hagiwara A, Hori M, Fukunaga I, Andica C, Maekawa T, Aoki S. Reduced visualization of cerebral infarction on diffusion-weighted images with short diffusion times. Neuroradiology, 2018; 60: 979–82. [PubMed: 30051336]

Budde MD, Frank JA. Neurite beading is sufficient to decrease the apparent diffusion coefficient after ischemic stroke. Proceedings of the National Academy of Sciences, 2010; 107: 14472–7.

Burcaw LM, Fieremans E, Novikov DS. Mesoscopic structure of neuronal tracts from time-dependent diffusion. NeuroImage, 2015; 114: 18–37. [PubMed: 25837598]

By S, Smith SA, Schilling KG, Weinberg Q, Devan SP, Bagnato FR, Xu J. Oscillating Gradient Spin Echo (OGSE) Diffusion Tensor Imaging of the Human Spinal Cord: Application to Multiple Sclerosis Proceedings of the 26th Annual Meeting of ISMRM: Paris, France, 2019: 953.

Callaghan PT, Stepisnik J. Frequency-Domain Analysis of Spin Motion Using Modulated-Gradient NMR. J Magn Reson Ser A, 1995; 117: 118–22.

Author Manuscript Author Manuscript Author Manuscript Author Manuscript

Chenevert TL, Galban CJ, Ivancevic MK, Rohrer SE, Londy FJ, Kwee TC, Meyer CR, Johnson TD, Rehemtulla A, Ross BD. Diffusion coefficient measurement using a temperature-controlled fluid for quality control in multicenter studies. Journal of magnetic resonance imaging : JMRI, 2011; 34: 983–7. [PubMed: 21928310]

Clark CA, Hedehus M, Moseley ME. Diffusion time dependence of the apparent diffusion tensor in healthy human brain and white matter disease. Magnetic resonance in medicine, 2001; 45: 1126–9. [PubMed: 11378893]

Colvin DC, Jourquin J, Xu J, Does MD, Estrada L, Gore JC. Effects of intracellular organelles on the apparent diffusion coefficient of water molecules in cultured human embryonic kidney cells. Magnetic resonance in medicine, 2011a; 65: 796–801. [PubMed: 21337411]

Colvin DC, Loveless ME, Does MD, Yue Z, Yankeelov TE, Gore JC. Earlier detection of tumor treatment response using magnetic resonance diffusion imaging with oscillating gradients. Magnetic resonance imaging, 2011b; 29: 315–23. [PubMed: 21190804]

Colvin DC, Yankeelov TE, Does MD, Yue Z, Quarles C, Gore JC. New insights into tumor microstructure using temporal diffusion spectroscopy. Cancer Res, 2008; 68: 5941–7. [PubMed: 18632649]

Conturo TE, McKinstry RC, Akbudak E, Robinson BH. Encoding of anisotropic diffusion with tetrahedral gradients: a general mathematical diffusion formalism and experimental results. Magnetic resonance in medicine, 1996; 35: 399–412. [PubMed: 8699953]

Does MD, Parsons EC, Gore JC. Oscillating gradient measurements of water diffusion in normal and globally ischemic rat brain. Magnetic resonance in medicine, 2003; 49: 206–15. [PubMed: 12541239]

Drobnjak I, Zhang H, Ianus A, Kaden E, Alexander DC. PGSE, OGSE, and sensitivity to axon diameter in diffusion MRI: Insight from a simulation study. Magnetic resonance in medicine, 2016; 75: 688–700. [PubMed: 25809657]

Engström M, Skare S. Diffusion-weighted 3D multislab echo planar imaging for high signal-to-noise ratio efficiency and isotropic image resolution. Magnetic resonance in medicine, 2013; 70: 1507–14. [PubMed: 23359357]

Fordham E, Mitra P, Latour L. Effective diffusion times in multiple-pulse PFG diffusion measurements in porous media. Journal of Magnetic Resonance, Series A, 1996; 121: 187–92.

Gao F, Shen X, Zhang H, Ba R, Ma X, Lai C, Zhang J, Zhang Y, Wu D. Feasibility of oscillating and pulsed gradient diffusion MRI to assess neonatal hypoxia-ischemia on clinical systems. Journal of cerebral blood flow and metabolism : official journal of the International Society of Cerebral Blood Flow and Metabolism, 2020: 271678X20944353.

Gore JC, Xu J, Colvin DC, Yankeelov TE, Parsons EC, Does MD. Characterization of tissue structure at varying length scales using temporal diffusion spectroscopy. NMR in biomedicine, 2010; 23: 745–56. [PubMed: 20677208]

Hattori T, Yuasa T, Aoki S, Sato R, Sawaura H, Mori T, Mizusawa H. Altered microstructure in corticospinal tract in idiopathic normal pressure hydrocephalus: comparison with Alzheimer disease and Parkinson disease with dementia. AJNR. American journal of neuroradiology, 2011; 32: 1681–7. [PubMed: 21816921]

Hennel F, Michael ES, Pruessmann KP. Improved gradient waveforms for oscillating gradient spin-echo (OGSE) diffusion tensor imaging. NMR in biomedicine, 2020: e4434. [PubMed: 33124071]

Hong X, Thomas Dixon W. Measuring diffusion in inhomogeneous systems in imaging mode using antisymmetric sensitizing gradients. J Magn Reson, 1992; 99: 561–70.

Hormuth DA 2nd, Sorace AG, Virostko J, Abramson RG, Bhujwalla ZM, Enriquez-Navas P, Gillies R, Hazle JD, Mason RP, Quarles CC, Weis JA, Whisenant JG, Xu J, Yankeelov TE. Translating preclinical MRI methods to clinical oncology. Journal of magnetic resonance imaging : JMRI, 2019.

Hosey TP, Harding SG, Green HA, Ansorge RE, Carpenter TA. Diffusion Tensor Imaging, Using Oscillating Gradients to Probe Short Diffusion Times, in the Human Brain Proceedings 11th Scientific Meeting, International Society for Magnetic Resonance in Medicine: Toronto, Canada, 2003: 2123.

Author Manuscript Author Manuscript Author Manuscript Author Manuscript

Ianus A, Siow B, Drobnjak I, Zhang H, Alexander DC. Gaussian phase distribution approximations for oscillating gradient spin echo diffusion MRI. J Magn Reson, 2013; 227: 25–34. [PubMed: 23261952]

Iima M, Yamamoto A, Kataoka M, Yamada Y, Omori K, Feiweier T, Togashi K. Time-dependent diffusion MRI to distinguish malignant from benign head and neck tumors. Journal of magnetic resonance imaging : JMRI, 2019; 50: 88–95. [PubMed: 30578563]

Ikeda M, Oka Y. The relationship between nerve conduction velocity and fiber morphology during peripheral nerve regeneration. Brain and behavior, 2012; 2: 382–90. [PubMed: 22950042]

Irie R, Kamiya K, Hori M, Suzuki M, Kamagata K, Maekawa T, Fujita S, Takenaka Y, Fukunaga I, Nakajima M, Miyajima M, Murata K, Aoki S. Evaluating microstructure of the corticospinal tract in normal pressure hydrocephalus with diffusion MRI using oscillating gradient spin-echo Proceedings of the 27th Annual Meeting of ISMRM: Montreal, Canada, 2019: 343.

Jiang X, Li H, Xie J, McKinley ET, Zhao P, Gore JC, Xu J. In vivo imaging of cancer cell size and cellularity using temporal diffusion spectroscopy. Magnetic resonance in medicine, 2017; 78: 156–64. [PubMed: 27495144]

Jiang X, Li H, Xie J, Zhao P, Gore JC, Xu J. Quantification of cell size using temporal diffusion spectroscopy. Magnetic resonance in medicine, 2016a; 75: 1076–85. [PubMed: 25845851]

Jiang X, Li H, Zhao P, Xie J, Khabele D, Xu J, Gore JC. Early detection of treatment-induced mitotic arrest using temporal diffusion magnetic resonance spectroscopy. Neoplasia, 2016b; 18: 387–97. [PubMed: 27292027]

Jiang X, McKinley ET, Xie J, Li H, Xu J, Gore JC. In vivo magnetic resonance imaging of treatment-induced apoptosis. Scientific reports, 2019a; 9: 9540. [PubMed: 31266982]

Jiang X, Xu J, Gore JC. Mapping Hepatocyte Size In Vivo using Temporal Diffusion Spectroscopy MRI. Magn Reson Med (In press), 2020.

Jiang X, Xu J, Gore JC. Quantitative temporal diffusion spectroscopy as an early imaging biomarker of radiation therapeutic response in gliomas: A preclinical proof of concept. Adv Radiat Oncol, 2019b; 4: 367–76. [PubMed: 31011683]

Kaden E, Kelm ND, Carson RP, Does MD, Alexander DC. Multi-compartment microscopic diffusion imaging. NeuroImage, 2016; 139: 346–59. [PubMed: 27282476]

Kakkar LS, Bennett OF, Siow B, Richardson S, Ianus A, Quick T, Atkinson D, Phillips JB, Drobnjak I. Low frequency oscillating gradient spin-echo sequences improve sensitivity to axon diameter: An experimental study in viable nerve tissue. NeuroImage, 2018; 182: 314–28. [PubMed: 28774648]

Kershaw J, Leuze C, Aoki I, Obata T, Kanno I, Ito H, Yamaguchi Y, Handa H. Systematic changes to the apparent diffusion tensor of in vivo rat brain measured with an oscillating-gradient spin-echo sequence. NeuroImage, 2013; 70: 10–20. [PubMed: 23274188]

Lemberskiy G, Baete SH, Cloos MA, Novikov DS, Fieremans E. Validation of surface-to-volume ratio measurements derived from oscillating gradient spin echo on a clinical scanner using anisotropic fiber phantoms. NMR in biomedicine, 2017; 30.

Li H, Jiang X, Wang F, Xu J, Gore JC. Structural information revealed by the dispersion of ADC with frequency. Magnetic resonance imaging, 2015; 33: 1083–90. [PubMed: 26117695]

Li H, Kaden E, Alexander DC, Gore JC, Francesca BR, Xu J. Multi-compartment microscopic diffusion imaging with oscillating gradients: simulation validation and application in multiple sclerosis patients Proceedings of the 25th Annual Meeting of ISMRM: Honolulu, HI, USA, 2017: 283.

Li H, Xu J, Gore JC, Dortch RD. Rapid measurement of axon diameter and volume fraction in human peripheral nerve in vivo using temporal diffusion spectroscopy Proceedings of the ISMRM Diffusion Workshop: Lisbon, Portugal, 2016.

Lundell H, Sønderby CK, Dyrby TB. Diffusion weighted imaging with circularly polarized oscillating gradients. Magnetic resonance in medicine, 2015; 73: 1171–6. [PubMed: 24639209]

Maekawa T, Hori M, Murata K, Feiweier T, Andica C, Fukunaga I, Koshino S, Hagiwara A, Kamiya K, Kamagata K, Wada A, Abe O, Aoki S. Choroid plexus cysts analyzed using diffusion-weighted imaging with short diffusion-time. Magnetic resonance imaging, 2019; 57: 323–7. [PubMed: 30605722]

Author Manuscript Author Manuscript Author Manuscript Author Manuscript

Maekawa T, Hori M, Murata K, Feiweier T, Fukunaga I, Andica C, Hagiwara A, Kamagata K, Koshino S, Abe O, Aoki S. Changes in the ADC of diffusion-weighted MRI with the oscillating gradient spin-echo (OGSE) sequence due to differences in substrate viscosities. Japanese journal of radiology, 2018; 36: 415–20. [PubMed: 29700795]

Malyarenko DI, Ross BD, Chenevert TL. Analysis and correction of gradient nonlinearity bias in apparent diffusion coefficient measurements. Magnetic resonance in medicine, 2014; 71: 1312–23. [PubMed: 23794533]

Mercredi M, Vincent TJ, Bidinosti CP, Martin M. Assessing the accuracy of using oscillating gradient spin echo sequences with AxCaliber to infer micron-sized axon diameters. Magma (New York, N.Y.), 2017; 30: 1–14.

Mitra PP, Sen PN, Schwartz LM, Le Doussal P. Diffusion propagator as a probe of the structure of porous media. Phys Rev Lett, 1992; 68: 3555–8. [PubMed: 10045734]

Neuman CH. Spin-echo of spins diffusing in a bounded medium. J Chem Phys, 1974; 60: 4508–11.

Novikov DS, Fieremans E, Jensen JH, Helpern JA. Random walk with barriers. Nat Phys, 2011; 7: 508–14. [PubMed: 21686083]

Novikov DS, Fieremans E, Jespersen SN, Kiselev VG. Quantifying brain microstructure with diffusion MRI: Theory and parameter estimation. NMR in biomedicine, 2019; 32: e3998. [PubMed: 30321478]

Novikov DS, Jensen JH, Helpern JA, Fieremans E. Revealing mesoscopic structural universality with diffusion. Proc Natl Acad Sci U S A, 2014; 111: 5088–93. [PubMed: 24706873]

Novikov DS, Kiselev VG. Surface-to-volume ratio with oscillating gradients. J Magn Reson, 2011; 210: 141–5. [PubMed: 21393035]

Novikov DS, Kiselev VG, Jespersen SN. On modeling. Magnetic resonance in medicine, 2018; 79: 3172–93. [PubMed: 29493816]

Parsons EC Jr., Does MD, Gore JC. Temporal diffusion spectroscopy: theory and implementation in restricted systems using oscillating gradients. Magnetic resonance in medicine, 2006; 55: 75–84. [PubMed: 16342147]

Portnoy S, Flint JJ, Blackband SJ, Stanisz GJ. Oscillating and pulsed gradient diffusion magnetic resonance microscopy over an extended b-value range: implications for the characterization of tissue microstructure. Magnetic resonance in medicine, 2013; 69: 1131–45. [PubMed: 22576352]

Reynaud O Time-Dependent Diffusion MRI in Cancer: Tissue Modeling and Applications. Frontiers in Physics, 2017; 5.

Reynaud O, Winters KV, Hoang DM, Wadghiri YZ, Novikov DS, Kim SG. Pulsed and oscillating gradient MRI for assessment of cell size and extracellular space (POMACE) in mouse gliomas. NMR in biomedicine, 2016; 29: 1350–63. [PubMed: 27448059]

Schachter M, Does MD, Anderson AW, Gore JC. Measurements of restricted diffusion using an oscillating gradient spin-echo sequence. J Magn Reson, 2000; 147: 232–7. [PubMed: 11097814]

Setsompop K, Kimmlingen R, Eberlein E, Witzel T, Cohen-Adad J, McNab JA, Keil B, Tisdall MD, Hoecht P, Dietz P, Cauley SF, Tountcheva V, Matschl V, Lenz VH, Heberlein K, Potthast A, Thein H, Van Horn J, Toga A, Schmitt F, Lehne D, Rosen BR, Wedeen V, Wald LL. Pushing the limits of in vivo diffusion MRI for the Human Connectome Project. NeuroImage, 2013; 80: 220–33. [PubMed: 23707579]

Stejskal EO. Use of spin echoes in a pulsed magnetic-field gradient to study anisotropic restricted diffusion and flow. J Chem Phys, 1965; 43: 3597–603.

Stejskal EO, Tanner JE. Spin diffusion measurements - spin echoes in presence of a time-dependent field gradient. J Chem Phys, 1965; 42: 288–92.

Stepisnik J Analysis of NMR self-diffusion measurements by a density-matrix calculation. Physica B, 1981; 104: 350–64.

Stepisnik J Time-dependent self-diffusion by NMR spin-echo. Physica B, 1993; 183: 343–50.

Sukstanskii AL. Exact analytical results for ADC with oscillating diffusion sensitizing gradients. J Magn Reson, 2013; 234: 135–40. [PubMed: 23876779]

Tan ET, Shih RY, Mitra J, Sprenger T, Hua Y, Bhushan C, Bernstein MA, McNab JA, DeMarco JK, Ho VB, Foo TKF. Oscillating diffusion-encoding with a high gradient-amplitude and high slew-rate

Author Manuscript Author Manuscript Author Manuscript Author Manuscript

head-only gradient for human brain imaging. Magnetic resonance in medicine, 2020; 84: 950–65. [PubMed: 32011027]

Tanner JE. Self diffusion of water in frog muscle. Biophysical journal, 1979; 28: 107–16. [PubMed: 318065]

Tanner JE, Stejskal EO. Restricted self-diffusion of protons in colloidal systems by pulsed-gradient spin-echo method. J Chem Phys, 1968; 49: 1768–77.

Tétreault P, Harkins KD, Baron CA, Stobbe R, Does MD, Beaulieu C. Diffusion time dependency along the human corpus callosum and exploration of age and sex differences as assessed by oscillating gradient spin-echo diffusion tensor imaging. NeuroImage, 2020; 210: 116533. [PubMed: 31935520]

Van AT, Holdsworth SJ, Bammer R. In vivo investigation of restricted diffusion in the human brain with optimized oscillating diffusion gradient encoding. Magnetic resonance in medicine, 2014; 71: 83–94. [PubMed: 23447055]

Vos SB, Tax CM, Luijten PR, Ourselin S, Leemans A, Froeling M. The importance of correcting for signal drift in diffusion MRI. Magnetic resonance in medicine, 2017; 77: 285–99. [PubMed: 26822700]

Warach S, Gaa J, Siewert B, Wielopolski P, Edelman RR. Acute human stroke studied by whole brain echo planar diffusion-weighted magnetic resonance imaging. Annals of Neurology: Official Journal of the American Neurological Association and the Child Neurology Society, 1995; 37: 231–41.

Wu D, Liu D, Hsu YC, Li H, Sun Y, Qin Q, Zhang Y. Diffusion-prepared 3D gradient spin-echo sequence for improved oscillating gradient diffusion MRI. Magnetic resonance in medicine, 2020.

Wu D, Martin LJ, Northington FJ, Zhang J. Oscillating-gradient diffusion magnetic resonance imaging detects acute subcellular structural changes in the mouse forebrain after neonatal hypoxia-ischemia. Journal of cerebral blood flow and metabolism : official journal of the International Society of Cerebral Blood Flow and Metabolism, 2019; 39: 1336–48. [PubMed: 29436246]

Wu D, Martin LJ, Northington FJ, Zhang J. Oscillating gradient diffusion MRI reveals unique microstructural information in normal and hypoxia-ischemia injured mouse brains. Magnetic resonance in medicine, 2014a; 72: 1366–74. [PubMed: 25168861]

Wu D, Zhang J. The Effect of Microcirculatory Flow on Oscillating Gradient Diffusion MRI and Diffusion Encoding with Dual-Frequency Orthogonal Gradients (DEFOG). Magnetic resonance in medicine, 2017; 77: 1583–92. [PubMed: 27080566]

Wu Y, Zhu YJ, Tang QY, Zou C, Liu W, Dai RB, Liu X, Wu EX, Ying L, Liang D. Accelerated MR diffusion tensor imaging using distributed compressed sensing. Magnetic resonance in medicine, 2014b; 71: 763–72. [PubMed: 23494999]

Xu J, Attia A, Arlinghaus LR, Kirschner AN, Osmundson EC, Kang H, Luo G. Selective Size Imaging using Filters via diffusion Times (SSIFT): A new contrast-free highly specific MR cancer imaging method Proceedings of the 26th Annual Meeting of ISMRM: Paris, France, 2017: 953.

Xu J, Attia A, Arlinghaus LR, Kirschner AN, Osmundson EC, Kang H, Luo G. Selective Size Imaging using Filters via diffusion Times (SSIFT): A new contrast-free highlyspecific MR cancer imaging method. Proceedings of the 27th Annual Meeting of ISMRM: Paris, France, 2019: 953.

Xu J, Does MD, Gore JC. Dependence of temporal diffusion spectra on microstructural properties of biological tissues. Magnetic resonance imaging, 2011a; 29: 380–90. [PubMed: 21129880]

Xu J, Does MD, Gore JC. Quantitative characterization of tissue microstructure with temporal diffusion spectroscopy. J Magn Reson, 2009a; 200: 189–97. [PubMed: 19616979]

Xu J, Does MD, Gore JC. Sensitivity of MR diffusion measurements to variations in intracellular structure: effects of nuclear size. Magnetic resonance in medicine, 2009b; 61: 828–33. [PubMed: 19205020]

Xu J, Jeong H-K, Does MD, Anderson AW, Chen L-M, Gore JC. Dependence of fractional anisotropy on diffusion time: a frequency-domain analysis using temporal diffusion spectroscopy Proceedings of the 18th Annual Meeting of ISMRM: Stockholm, Sweden, 2010: 4038.

Xu J, Jiang X, Li H, Arlinghaus LR, McKinley ET, Devan SP, Hardy BM, Xie J, Kang H, Chakravarthy AB, Gore JC. Magnetic resonance imaging of mean cell size in human breast tumors. Magnetic resonance in medicine, 2020; 83: 2002–14. [PubMed: 31765494]

Author Manuscript Author Manuscript Author Manuscript Author Manuscript

Xu J, Li H, Harkins KD, Jiang X, Xie J, Kang H, Does MD, Gore JC. Mapping mean axon diameter and axonal volume fraction by MRI using temporal diffusion spectroscopy. NeuroImage, 2014; 103: 10–9. [PubMed: 25225002]

Xu J, Li H, Li K, Harkins KD, Jiang X, Xie J, Kang H, Dortch RD, Anderson AW, Does MD, Gore JC. Fast and simplified mapping of mean axon diameter using temporal diffusion spectroscopy. NMR in biomedicine, 2016; 29: 400–10. [PubMed: 27077155]

Xu J, Li K, Smith RA, Waterton JC, Zhao P, Chen H, Does MD, Manning HC, Gore JC. Characterizing tumor response to chemotherapy at various length scales using temporal diffusion spectroscopy. PLoS One, 2012; 7: e41714. [PubMed: 22911846]

Xu J, Xie J, Jourquin J, Colvin DC, Does MD, Quaranta V, Gore JC. Influence of cell cycle phase on apparent diffusion coefficient in synchronized cells detected using temporal diffusion spectroscopy. Magnetic resonance in medicine, 2011b; 65: 920–6. [PubMed: 21413058]

Zhang H, Schneider T, Wheeler-Kingshott CA, Alexander DC. NODDI: practical in vivo neurite orientation dispersion and density imaging of the human brain. NeuroImage, 2012; 61: 1000–16. [PubMed: 22484410]

Author Manuscript Author Manuscript Author Manuscript Author Manuscript

Highlights

- The OGSE sequence with short diffusion times is sensitive to small length scales
- The OGSE sequence has been translated to clinical MRI systems for patients
- More technical improvements and clinical applications are needed for OGSE imaging

Author Manuscript Author Manuscript Author Manuscript Author Manuscript

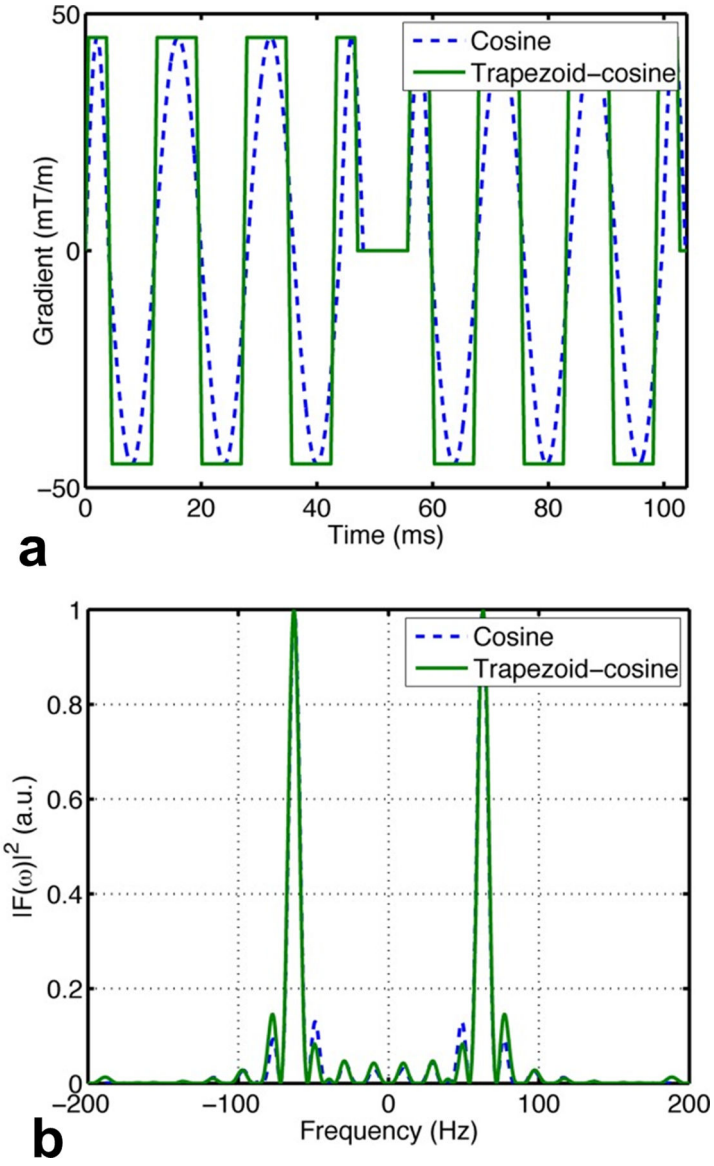

Fig. 1.

Comparison between the cosine and trapezoid-cosine (a) gradient waveforms and (b) corresponding encoding spectra $|F(\omega)|^2$. The figure is reprinted with permission from (Van et al., 2014).

Author Manuscript Author Manuscript Author Manuscript Author Manuscript

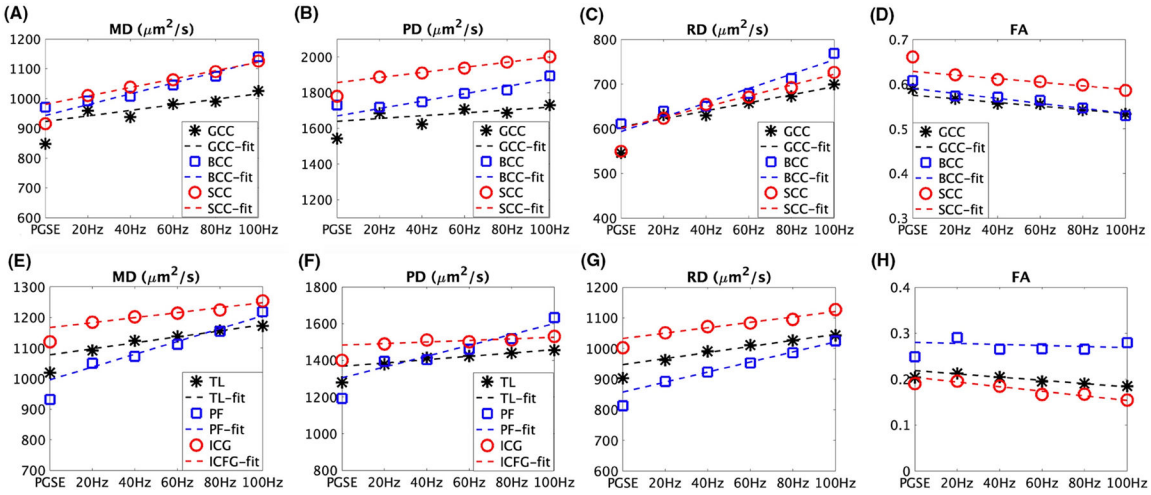

Fig. 2.

Representative diffusion time dependence of DTI metrics: MD (mean diffusivity), PD (parallel diffusivity), RD (radial diffusivity), and FA (fractional anisotropy) in three white matter regions and three gray matter regions of a healthy subject. GCC: genu, BCC: body, and SCC: splenium of the corpus callosum. TL: temporal lobes. PF: posterior fossa, and ICG: insula/cingulate gyri. The figure is reprinted with permission from (Tan et al., 2020).

Author Manuscript Author Manuscript Author Manuscript Author Manuscript

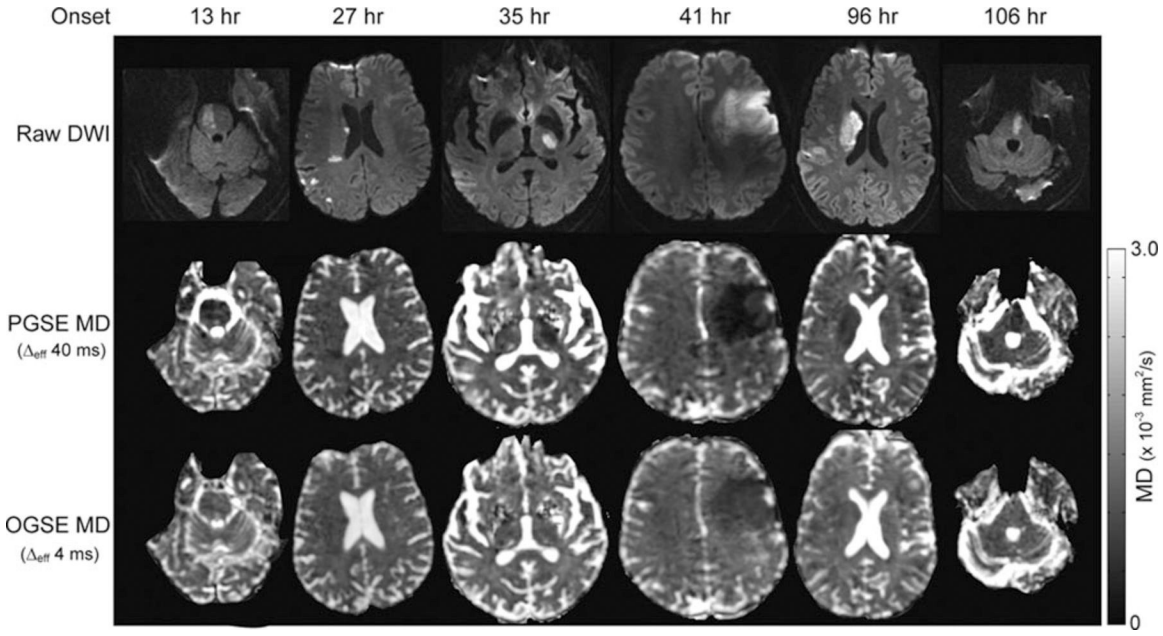

Fig. 3.

Representative images of raw dMRI, PGSE MD, and OGSE MD maps at multiple time points post-onset of ischemic stroke. The figure is reprinted with permission from (Baron et al., 2015).

Author Manuscript Author Manuscript Author Manuscript Author Manuscript

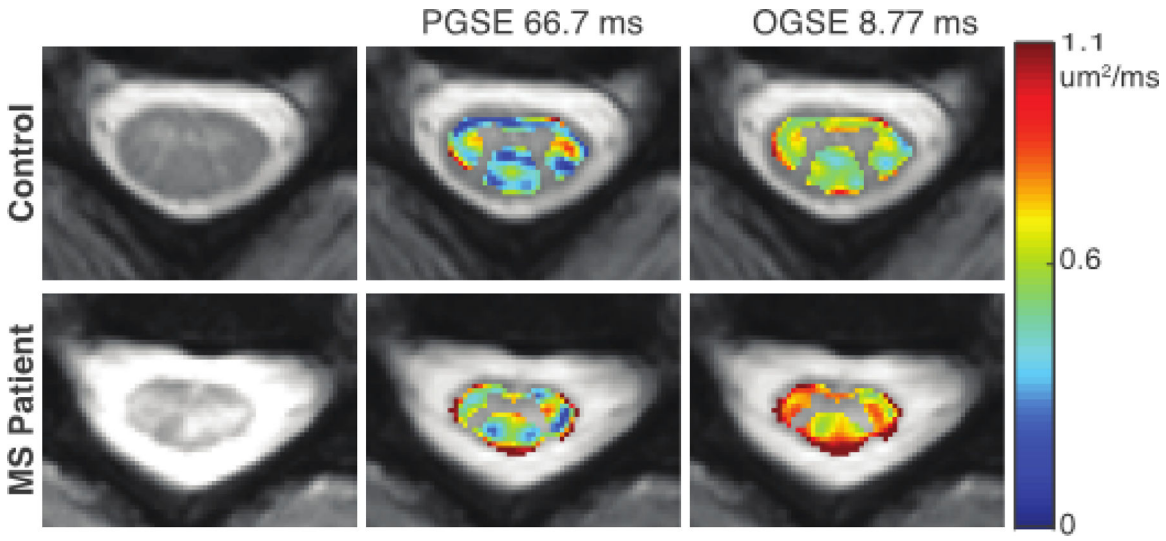

Fig. 4.

Comparison of RD maps in healthy control (top) and MS patient (bottom). From left to right, the anatomical image, RD map acquired with an effective diffusion time of 66.7 ms, and RD map acquired with an effective diffusion time of 8.77 ms are shown. A larger difference is observed between the healthy control and MS patient with the shorter diffusion times achievable with OGSE. The figure is reprinted with permission from (By et al., 2019).

Author Manuscript Author Manuscript Author Manuscript Author Manuscript

Table 1

A summary of representative protocols and hardware in previous OGSE imaging studies in humans.

Studies	Scanner	Maximum gradient strength G_{max} and slew rate SR_{max}	Gradient waveform used	Gradient duration δ and echo time TE	Maximum b and f achieved
Hosey et al. (Hosey et al., 2003)	Bruker MedSpec 300 3 T	G_{max} = 30 mT/m SR_{max} = 70 T/m/s	Sine	δ = 50 ms TE = 152 ms	b = 650 s/mm^2 f = 20 Hz
Van et al. (Van et al., 2014)	GE MR750 3 T	G_{max} = 50 mT/m SR_{max} = 200 T/m/s	Trapezoid-cosine	δ = 48 ms TE = 116 ms	b = 200 s/mm^2 f = 65 Hz
Baron et al. (Baron and Beaulieu, 2014)	Varian Unity Inova 4.7 T	G_{max} > 57.5 mT/m SR_{max} > 70 T/m/s	Trapezoid-cosine	δ = 41.2 ms TE = 110 ms	b = 300 s/mm^2 f = 50 Hz
Xu et al. (Xu et al., 2016)	Philips Achieva 3 T	G_{max} = 80 mT/m SR_{max} = 100 T/m/s	Trapezoid-cosine	δ = 50 ms TE = 124 ms	b = 400 s/mm^2 f = 40 Hz
Andica et al. (Andica et al., 2018)	Siemens MAGNETOM Prisma 3 T	G_{max} = 80 mT/m SR_{max} > 100 T/m/s	Trapezoid-sine	δ = 41.3 ms TE = 120 ms	b = 1500 s/mm^2 f = 50 Hz
Maekawa et al. (Maekawa et al., 2019)	Siemens MAGNETOM Prisma 3 T	G_{max} = 80 mT/m SR_{max} > 100 T/m/s	Trapezoid-cosine	δ = 33.3 ms TE = 120 ms	b = 1000 s/mm^2 f = 30 Hz
Xu et al. (Xu et al., 2020)	Philips Achieva 3 T	G_{max} = 80 mT/m SR_{max} = 100 T/m/s	Trapezoid-cosine	δ = 40 ms TE = 104 ms	b = 300 s/mm^2 f = 50 Hz
Arbabi et al. (Arbabi et al., 2020)	Siemens MAGNETOM Terra 7 T *	G_{max} = 80 mT/m SR_{max} = 350 T/m/s	Trapezoid-cosine	δ = 33.3 ms TE = 111 ms	b = 450 s/mm^2 f = 60 Hz
Tan et al. (Tan et al., 2020)	GE Signa MR750 3 T *	G_{max} = 200 mT/m SR_{max} = 500 T/m/s	Trapezoid-cosine	δ = 50 ms TE = 122 ms	b = 450 s/mm^2 f = 100 Hz

Author Manuscript Author Manuscript Author Manuscript Author Manuscript

Studies	Scanner	Maximum gradient strength G_{max} and slew rate SR_{max}	Gradient waveform used	Gradient duration δ and echo time TE	Maximum b and f achieved
Hennel et al. (Hennel et al., 2020)	Philips Achieva 3 T*	G_{max} = 200 mT/m SR_{max} = 600 T/m/s	Modified trapezoid-cosine	δ = ~40 ms ** TE = 120 ms	b = 975 s/mm^2 f = 75 Hz

* A head-only gradient coil insert was used.

** the gradient durations vary with different frequencies

J Neurosci Methods. Author manuscript; available in PMC 2023 April 24.